Building and Environment 205 (2021) 108278

Contents lists available at ScienceDirect

Building and Environment

journal homepage: www.elsevier.com/locate/buildenv

Estimating the impact of indoor relative humidity on SARS-CoV-2 airborne transmission risk using a new modification of the Wells-Riley model

Amar Aganovic [a,*], Yang Bi [b], Guangyu Cao [b], Finn Drangsholt [a], Jarek Kurnitski [c], Pawel Wargocki [d]

[a] Department of Automation and Process Engineering, UiT The Arctic University of Norway, Tromsø, Norway
[b] Department of Energy and Process Engineering, Norwegian University of Science and Technology - NTNU, Trondheim, Norway
[c] REHVA Technology and Research Committee, Tallinn University of Technology, Tallinn, Estonia
[d] Department of Civil Engineering, Technical University of Denmark, Copenhagen, Denmark

ARTICLE INFO

Keywords:
SARS-CoV-2
Virus airborne transmission
Ventilation
Relative humidity
Indoor environment

ABSTRACT

A novel modified version of the Wells-Riley model was used to estimate the impact of relative humidity (RH) on the removal of respiratory droplets containing the SARS-CoV-2 virus by deposition through gravitational settling and its inactivation by biological decay; the effect of RH on susceptibility to SARS-CoV-2 was not considered. These effects were compared with the removal achieved by increased ventilation rate with outdoor air. Modeling was performed assuming that the infected person talked continuously for 60 and 120 min. The results of modeling showed that the relative impact of RH on the infection risk depended on the ventilation rate and the size range of virus-laden droplets. A ventilation rate of 0.5 ACH, the change of RH between 20% and 53% was predicted to have a small effect on the infection risk, while at a ventilation rate of 6 ACH this change had nearly no effect. On the contrary, increasing the ventilation rate from 0.5 ACH to 6 ACH was predicted to decrease the infection risk by half which is remarkably larger effect compared with that predicted for RH. It is thus concluded that increasing the ventilation rate is more beneficial for reducing the airborne levels of SARS-CoV-2 than changing indoor RH.

Practical implications: The present results show that humidification to moderate levels of 40%–60% RH should not be expected to provide a significant reduction in infection risk caused by SARS-CoV-2, hence installing and running humidifiers may not be an efficient solution to reduce the risk of COVID-19 disease in indoor spaces. The results do however confirm that ventilation has a key role in controlling SARS-CoV-2 virus concentration in the air providing considerably higher benefits. The modified model developed in the present work can be used by public health experts, engineers, and epidemiologists when selecting different measures to reduce the infection risk from SARS-CoV-2 indoors allowing informed decisions concerning indoor environmental control.

1. Introduction

At the start of the pandemic in 2020, the recommendations related to infection control published by the World Health Organization (WHO) [1] acknowledged respiratory droplet transmission (>5μm) as the only mode of SARS-CoV-2 airborne transmission, while possible transmission by aerosols ($\leq$ 5 μm) was disputed considering the limited evidence available. These WHO recommendations have repeatedly come under strong criticism from numerous studies, arguing that microdroplets or aerosols $\leq$ 5 μm in size are small enough to remain suspended in the air and expose individuals at distances beyond 2 m from an infected person [2–6]. In support of these critics, the number of studies reporting samples positive for the SARS-CoV-2 genome (RNA) detected in central ventilation systems distant from patient areas was growing at the end of 2020 [7]. The transport mechanism of RNA SARS-CoV-2 found in these ventilation systems may not be reasonably explained by the droplet transmission of particles >5μm, due to their aerodynamic nature and high gravitational settling velocities. However, research has shown that even respiratory droplets with an initial size range up to 60–80 μm can travel 1–4 m from the mouth once they are in a dehydrated form after evaporation, depending on ambient air turbulence and relative humidity (RH) [8,9]. Contrary to previous beliefs, this finding implies that the virus can be transported by airborne particles >5 μm over much longer distances than specified by the conventional social distancing rules of 1–2 m [10]. Therefore, preventive measures in indoor environments should be based on control strategies that acknowledge the transmission

* Corresponding author.
E-mail address: amar.aganovic@uit.no (A. Aganovic).

https://doi.org/10.1016/j.buildenv.2021.108278
Received 3 July 2021; Received in revised form 16 August 2021; Accepted 18 August 2021
Available online 23 August 2021

of SARS-CoV-2 through airborne respiratory particles of all sizes. In this context, predictive mathematical models can be fundamental tools for planning effective prevention strategies based on a retrospective assessment of the numerous infection outbreaks that have occurred during the SARS-CoV-2 pandemic.

The most commonly applied epidemiological model for evaluating the airborne transmission dynamics of infectious diseases in confined spaces is based on the infection risk model originally developed by Riley et al., also known as the Wells-Riley model [11]. The model is based on the 'quantum of infection' concept, as proposed by Wells [12], defined as the number of infectious droplet nuclei or the infectious dose required to infect $1-\frac{1}{e}$ (i.e., 63.2%) of susceptible persons in an enclosed space. The Wells–Riley model assumes a control volume filled with well-mixed room air with a source term representing the steady-state quanta generation rate from infected persons and a sink term represented by a constant ventilation rate that removes the quanta concentration. Although the Wells–Riley model has been extensively used to analyze infectious disease outbreaks, such as TB risk probability in a confined space [13], its original version has several limitations, some of which are discussed in the following text. The original Wells-Riley model is based on the assumption of steady-state quanta, and subsequent modifications were made to overcome this limitation. Gammaitoni and Nucci [14] introduced a model capable of incorporating non–steady-state quanta levels. In particular, the differential equation for the change in quanta over time in a control volume as well as the initial conditions allowed for the evaluation of quanta concentration in an indoor environment at a certain time interval. However, as in the original Wells-Riley model, the Gammaitoni and Nucci model [15] also considered the ventilation rate as the only removal/sink term in the equation. Therefore, the equation has been upgraded in later models to incorporate many other removal mechanisms and control measures that can affect the infection risk, i.e., biological decay of the airborne pathogen and the deposition loss of the infectious particles [14]. To consider these two influencing factors using the Wells-Riley model, knowledge of the deposition and viability losses during the outbreak case is required.

To adapt these equations for specific assessments of airborne SARS-CoV-2 transmission risk in enclosed spaces, a model developed by Buonanno et al. [16] in which a novel term for the emission source was introduced, was implemented in Gammaitoni and Nucci's equation [14]. The novel source term calculates the quanta emission rate data of SARS-CoV-2 or the viral load emitted by an infected individual as a function of different respiratory activities, respiratory parameters, and activity levels based on droplet size measurements by Morawska et al. [17]. Buonanno's model also expands the removal term of Gammaitoni and Nucci's equation by considering both the airborne decay of SARS-CoV-2 and the deposition loss of infectious particles. However, both of the removal terms in this model can only be calculated for one specific environmental condition, i.e., RH. This is a likely limitation of the model, as RH may affect airborne SARS-CoV-2 transmission via both the deposition loss and airborne decay of infectious droplets [18,19].

Several studies have indicated that RH and temperature have a significant influence on the incidence of COVID-19 in a certain location [20–22]; i.e., these studies share common findings that colder and drier climates may increase the incidence of COVID-19. Although several recent experimental studies have been linking the survival of the SARS-CoV-2 virus in aerosols under various RH and temperature conditions [23–25], the precise nature of the relationships is much less clear. In contrast, the relationship between deposition loss by gravitational settling and RH is clear: the deposition loss of infectious particles is determined by the droplets settling or terminal velocity, which itself is dependent on droplet size. When released from the respiratory tract (assumed to have ~99.5% RH), droplets experience rapid evaporation and shrinkage upon encountering the unsaturated ambient atmosphere. The ultimate size of a droplet depends on ambient humidity, and size determines aerodynamic behavior and whether the droplet will settle to the ground quickly or remain suspended in the air long enough to possibly cause a secondary infection. Due to low RH, the droplets that evaporate to a smaller size could lead to a greater airborne suspension time of viral droplets and ultimately, they could be transported farther, depending on ventilation conditions. The dependence of the equilibrium size of an aqueous droplet containing dry solutes on RH is described by one of the fundamental interpretations of equilibrium thermodynamics, also known as the Köhler theory [26]. Therefore, without incorporating the impact of RH, current modifications of the Wells-Riley models are limited to only one specific RH assessment of the removal terms by inactivation and gravitational settling.

The wide range of RH values, as defined by existing building regulations design criteria for humidity in both the U.S. (RH < 65% as per ASHRAE 2013b [27]) and Europe (20 < RH < 70% used for existing buildings as per EN 16798–1 [28]) together with the intensified sensitivity of nasal systems and mucous membranes to infections at low RH of 10–20% [29,30], emphasizes the need for incorporating the variability of RH values in epidemiological models for a more accurate prediction of airborne transmission risks of SARS-CoV-2 in confined spaces. Consequently, by addressing these factors, a novel model for calculating the infection risk of airborne infectious transmission of SARS-CoV-2 as a function of RH is introduced in the present paper. To advance a mechanistic understanding of the role of RH (RH) in aerosol transmission, we model the change in the size of respiratory droplets and aerosols and SARS-CoV-2 airborne decay at RHs ranging from 20% to 83.5%. Based on these results, we further modeled the dynamics of droplets emitted from an infected person in an indoor environment to simulate the airborne transmission of SARS-CoV-2 viral load, considering removal by ventilation, deposition by gravitational settling, and biological decay of the SARS-CoV-2 virus in aerosols. The proposed model can support public health experts, engineers, and epidemiologists in obtaining a more comprehensive understanding of the impact of RH on the infection risk in indoor spaces.

2. Methodology

2.1. The modified Wells-Riley model for calculating infection risk as a function of RH

A schematic representation of the theoretical model assessing the impact of RH on the quanta emission rate of SARS-CoV-2 for infection risk assessment is shown in Fig. 1.

For this model, the following assumptions are made:

i) The room air is fully (ideal) mixed.
ii) No air recirculation by the ventilation system.
iii) The only emission source of SARS-CoV-2 is from the infected individual within the room who emits SARS-CoV-2 quanta at a constant rate.
iv) There are three removal mechanisms of the infectious quanta: deposition by gravitational settling, virus inactivation by biological decay, and ventilation without recirculation or exhaust to outdoor air.
v) The volumetric flow rates of outdoor and exhaust air are assumed to be equal and constant for the time interval of the analysis.
vi) Infectious respiratory airborne droplets quickly become evenly distributed throughout the room air.
vii) No virus-laden airborne particles enter from the outside ($n_{out} = 0$).
viii) There is no prior source of quanta in the space.
ix) Filtration of the exhalation droplets was not performed using a face mask.
x) The viral content of a saliva droplet produced by an infected person is proportional to its initial volume [31].
xi) The indoor RH does not change due to the vapor generated by human breathing and evaporation processes.

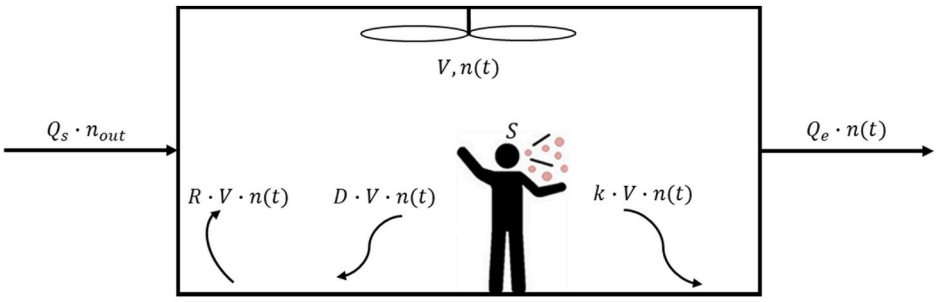

Fig. 1. Schematic representation of a simple indoor air mass-balance model in a well-mixed room, including a source term S and removal mechanisms by ventilation, inactivation *k*, deposition by settling *D,* and resuspension *R*.

xii) Resuspension rate *R* is neglected in the model ($R \approx 0$).
xiii) The removal rate due to absorption in the respiratory tract by the infected person is neglected in this model.
xiv) There is no simulated sunlight indoors (ultraviolet B solar irradiance ≈0 W/m^2).
xv) The infection risk calculation does not account for the potential effect of RH on human response in terms of susceptibility to infection.

The mass balance model for a well-mixed indoor mechanically ventilated room model can be represented by the following differential equation:

$$V \cdot \frac{dn(t)}{dt} = S + Q_S \cdot n_{out} - Q_e \cdot n(t) - k \cdot n(t) \cdot V - D \cdot V \cdot n(t) - R \cdot V \cdot n(t) \quad (1)$$

V – volume of room, m^3
$n\ (t)$ – quanta concentration in the indoor environment at the time (t), $\frac{quanta}{m^3}$
S – quanta source emission rate from infected persons (source), $\frac{quanta}{h}$
$Q_s = Q_e = Q$ – supply and exhaust airflow rate, $\frac{m^3}{h}$
$n_{out} = 0$ - quanta concentration outdoors, $\frac{quanta}{h}$
k – virus inactivation rate, $\frac{1}{h}$
D – deposition rate, $\frac{1}{h}$
R-resuspension rate, $\frac{1}{h}$

To solve equation (1) in the form of a first-order differential equation $\frac{dn(t)}{dt} + n(t) \cdot a = b$, it may be rewritten as follows:

$$\frac{dn(t)}{dt} + n(t) \cdot \left(\frac{Q}{V} + D + k\right) = \frac{S}{V} \quad (2)$$

The unique solution of (2) is:

$$n(t) = n_0 \cdot exp\left[- \left(\frac{Q}{V} + D + k\right) t \right] + \frac{S}{V} \cdot \left\{ \frac{1}{\frac{Q}{V} + D + k} - \frac{1}{\frac{Q}{V} + D + k} \cdot exp\left[- \left(\frac{Q}{V} + D + k\right) t \right] \right\} \quad (3)$$

where n_0 is the initial quanta concentration ($\frac{quanta}{m^3}$) at time t = 0.

To perform calculations with (3) to predict indoor concentrations of quanta at time *t*, appropriate expressions for the source term *S*, deposition rate *D* and inactivation rate *k* must be determined.

2.1.1. The source term S

The pollutant source emission rate *S* is defined as the quanta emission rate of SARS-CoV-2 generated by infected persons and can be defined by Ref. [15]:

$$S = I \cdot c_v \cdot c_i \cdot IR \cdot \sum_{i=1}^{n} (N_i \cdot V_i) \quad (4)$$

I – number of infected persons, -
c_v – viral load in the sputum, $\frac{RNA}{ml}$
c_i – conversion factor is defined as the ratio between one infectious quantum and the infectious dose expressed in viral RNA copies (quanta/RNA). Schijven et al. [32] developed a dose-response relationship that estimated an average of 1440 viral copies per infectious dose of SARS-CoV-2. Therefore, we estimated $c_i = \frac{1\ quanta}{1440\ RNA} = 6.94 \cdot 10^{-4} \frac{quanta}{RNA}$
IR – ($\frac{m^3}{h}$) – inhalation rate, i.e., the product of breathing (N_{br}) and tidal volume (V_{br}) –are both functions of the activity level of the infected subject. The inhalation rates for resting and standing averaged between males and females are equal to 0.49 and 0.54 $\frac{m^3}{h}$, respectively [33].
N_i - droplet number concentration in the ith bin, $\frac{particles}{cm^3}$
V_i – the mean volume of a single droplet (mL) in the ith bin.

$$V_i\ (D) = \frac{\pi \cdot \left(D_{max}^4 - D_{min}^4\right)}{24 \cdot (D_{max} - D_{min})} \quad (5)$$

where D_{max} and D_{min} denote the bin's lower and upper diameter values, according to Nicas [34]. *i*– size bin of the droplet distribution.

The size distribution for talking is determined experimentally by the works of Morawska et al. [17] for droplet aerosols $\leq 2\ \mu m$ and Chao et al. [35] for respiratory droplets $\geq 2\ \mu m$: both studies measured the size distribution of droplets for talking/voice counting at a distance of 10 mm from the participant's mouth opening. Therefore, the measured concentration of droplets represents the original size of the droplets at the mouth opening or the mass equivalent diameter of the particle D_{eq}(m) at the temperature and RH in the respiratory tract (37 °*C* and RH = 99.5%). The total volume of droplets was calculated by multiplying the droplet number distribution by the mean volume corresponding to each diameter in the size distribution. The size droplet distributions for each bin (i) are shown in Table A1 in the Supplementary Material attached online (A1).

2.1.2. Virus inactivation rate/biological decay constant k

To characterize the impact of relative humidity on the inactivation rate, experimental data [23–25] on the survival time of SARS-CoV-2 in aerosols were aggregated for measured values of k (min^{-1}) at RH = 20% (Num 1–3), 37% (Num 4–5), 53% (Num 6–9), 70% (Num 10–12) and 83.5% (Num 13–14) at T = 20–20.5 °C from Table 1 to Fig. 2:

Table 1
Biological decay constant, k as reported in experimental studies [23–25].

Source	Artificial Saliva	Relative humidity (%)	Mean Temperature (°C)	The decay constant, k min^{-1})	Number
Schuit et al. [24]	Yes	20.0	20	0.01000	1
Schuit et al. [24]	No	20.0	20	0.01500	2
Dabisch et al. [23]	Yes	20.0	20	0.00600	3
Schuit et al. [24]	Yes	37.0	20	−0.00250	4
Schuit et al. [24]	No	37.0	20	0.01300	5
Schuit et al. [24]	Yes	53.0	20	0.00800	6
Schuit et al. [24]	No	53.0	20	0.00750	7
Smither et al. [25]	Yes	55.0	20.5	0.01590	8
Smither et al. [25]	No	55.5	20.5	0.00910	9
Schuit et al. [24]	Yes	70.0	20	0.01750	10
Schuit et al. [24]	No	70.0	20	0.01500	11
Dabisch et al. [23]	Yes	70.0	20	0.01700	12
Smither et al. [25]	Yes	81.0	20.5	0.04000	13
Smither et al. [25]	No	86.0	20.5	0.02270	14

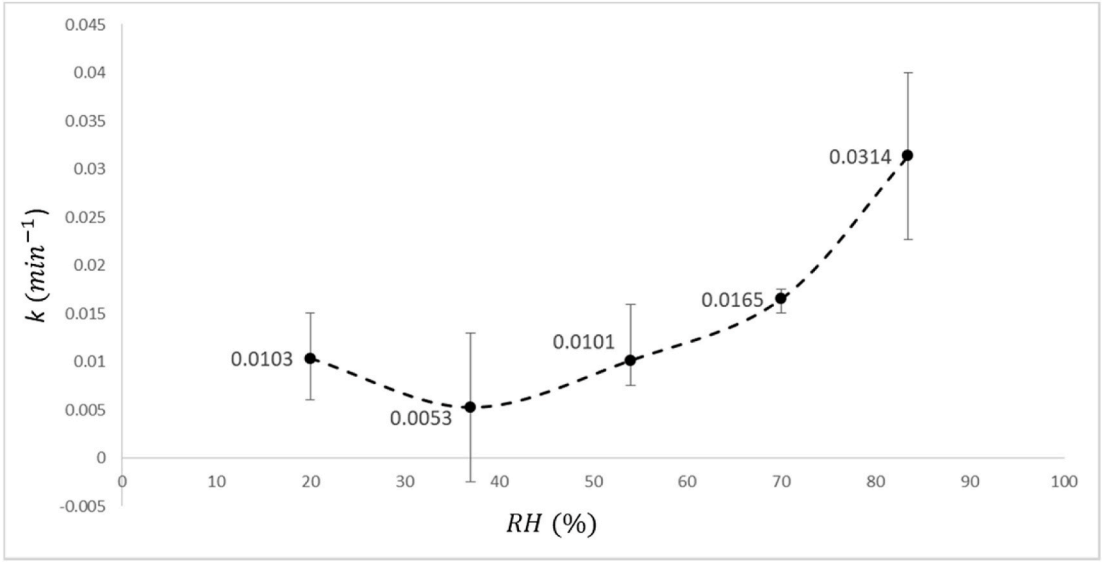

Fig. 2. Mean, min, and max IAV inactivation rates (k) for each RH were derived based on experimental data adapted from Dabisch et al. [23], Schuit et al. [24], and Smither et al. [25], as presented in Table 1.

2.1.3. The deposition rate D

The deposition rate D of a virus-laden droplet can be expressed as follows:

$$D = \frac{v_s}{H_{person}} \tag{6}$$

H_{person} – average height of the infected person(s), m

The gravitational settling velocity of the droplets v_s and $\frac{m}{s}$ can be determined from the following:

$$v_s = \sqrt{\frac{4 \cdot \rho_d \cdot g \cdot D_{eq}}{3 \cdot \rho_a \cdot C_{d,s}}} \tag{7}$$

g – gravitational acceleration, $\frac{m}{s^2}$
ρ_d – density of droplets, $\frac{kg}{m^3}$
ρ_a – density of air, $\frac{kg}{m^3}$
D_{eq} – the droplet equilibrium diameter, m

C_{ds} is the drag coefficient at sedimentation (−) and can be determined as one of the existing empirical expressions for $R_e < 2 \cdot 10^5$ [36]:

$$C_{ds} = \frac{24}{Re} \cdot \left(1 + 0.15 \cdot Re^{0.681}\right) + \frac{0.407}{1 + 8710 \cdot Re^{-1}} \tag{8}$$

C_{ds} depends on the droplets' Reynolds number:

$$R_e = \frac{\rho_a \cdot D_{eq} \cdot v_s}{\eta_d} \tag{9}$$

η_d – dynamic viscosity of air, $\frac{Pa}{s}$

This implies that the settling velocity v_s can only be calculated iteratively using equation (7). To perform the numerical iterations for the gravitational settling velocity from equation (8), the mass equivalent diameter of the particle D_{eq}(m) must be known for a specific RH value. In this manner, the mass equivalent diameter of the particle D_{eq} can be obtained from the Köhler theory [26], considering the two major respiratory fluid components in addition to water: inorganic salts and glycoproteins. We hereby assume respiratory fluid contains 8.8 g L^{-1}

NaCl to represent the inorganic components and 76 g L^{-1} of total proteins (TP) to approximate the organic components, as reported by Nicas et al. [34]. The relationship between the RH and equilibrium droplet diameter (D_{eq}) can be derived from the separate solute volume additivity (SS-VA) model for multi-component particles by Mikhailov et al. [37]. Their modeling results for particles consisting of 90% dry mass fraction fit the experimental data for the dehydration of mixed NaCl-dry mass solute particles well. Given the similar composition of respiratory fluid (89.6% TP in dry mass) to their NaCl-dry mass solute particles, the SS-VA model can be used to compute the equilibrium size for respiratory droplets [38].

The SS-VA model predicts the equilibrium RH with a specific droplet diameter (D_{eq}) to be as follows:

$$RH = \exp\left(\frac{4\cdot\sigma\cdot M_w}{\rho_d\cdot R\cdot T\cdot D_{eq}} - \frac{M_w}{\rho_w\cdot\left(\left(\frac{D_{eq}}{D_{m,s}}\right)^3 - 1\right)}\cdot\sum_y \frac{v_y\cdot\Phi_y\cdot\rho_y\cdot x_{s,y}}{M_y}\right) \tag{10}$$

the subscripts w and y refer to water and component y (either NaCl or TP), respectively

σ – surface tension of water, $\frac{N}{m}$

M_w – molar mass water, g/mol

M_y – molar mass of dry solutes (either NaCl or TP), $g/\ mol$

ρ_y – density of dry solutes (either NaCl or TP), g/mol

ρ_d – density of droplets, $\frac{kg}{m^3}$

ρ_w – density of water, $\frac{kg}{m^3}$

R – ideal gas constant, $\frac{J}{K\cdot mol}$

T – absolute temperature, K

$x_{s,y}$ is the mass fraction of component y in the dry solute, -

$D_{m,s}$ is the mass equivalent diameter of a particle consisting of dry solutes, m

v_y, the stoichiometric dissociation number of the component, -

Φ_y, - the molal or practical osmotic coefficient can be obtained from the following equation:

$$\Phi_s = 1 + \frac{g_{eff,y}^{-3}\cdot\left(3 - g_{eff,y}^{-6}\right)}{\left(3 - g_{eff,y}^{-3}\right)^2} \tag{11}$$

$g_{eff,y}$ is regarded as the volume fraction of the pure solute y in the reference solution and is calculated according to:

$$g_{eff,y} = \left(\frac{\rho_y}{\rho_s\cdot x_{s,y}}\cdot\left(\left(\frac{D_{eq}}{D_{m,s}}\right)^3 - 1\right) + 1\right)^{1/3} \tag{12}$$

The calculated equivalent dehydrated droplet diameter at five RH values: 20%, 37%, 53%, 70%, and 83.5%, for an original droplet size of 10 μm was observed to be constant within the indoor air temperature range of 20–25 $^\circ C$ for each RH level considered, as shown in Fig. 3. Therefore the case scenario simulations shown in the Results section below were performed for the temperature of $T = 20\ ^\circ C = 293K$.

The three removal terms due to ventilation $\left(\frac{Q}{V}\right)$, the aerosol deposition rate ($D = \frac{v_s}{H_{person}}$) and the viral inactivation rate (k) can be summed into one term called the infectious virus removal rate in the space investigated $IVRR$ (h^{-1}):

$$IVRR_i = \frac{Q}{V} + \frac{\sqrt{\frac{4\cdot\rho_d\cdot g\cdot D_{eq,i}}{3\cdot\rho_a\cdot C_{ds,i}}}}{H_{person}} + k \tag{13}$$

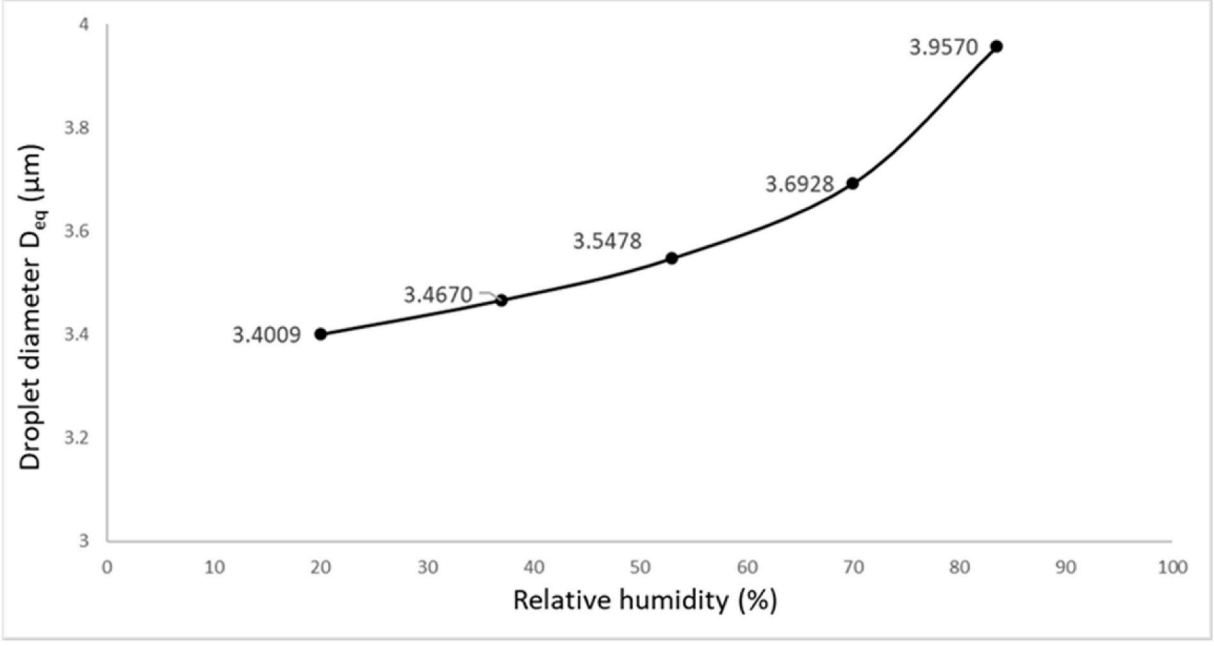

Fig. 3. Equivalent dehydrated droplet diameter at five RH values (RH = 20%, 37%, 53%, 70% and 83.5%) for an original droplet size of 10 μm the indoor air temperature range 20–25 $^\circ C$.

This allows for the final form to evaluate the quanta concentration in an indoor environment at time t, $n(t)$, as follows:

$$n(t) = \sum_{i=1}^{4} n_{0,i} \cdot e^{-(IVRR_i)\cdot t} + \frac{I \cdot c_v \cdot c_i \cdot IR \cdot \sum_{i=1}^{n} \left(N_{i,j} \cdot V_i\right)}{V} \cdot \left\{ \frac{1}{IVRR_i} - \frac{1}{IVRR_i} \cdot e^{-(IVRR_i)\cdot t} \right\} \Rightarrow$$

$$n(t) = \sum_{i=1}^{4} n_{0,i} \cdot e^{-(IVRR_i)\cdot t} + \frac{S}{V} \cdot \left\{ \frac{1}{IVRR_i} - \frac{1}{IVRR_i} \cdot e^{-(IVRR_i)\cdot t} \right\} \quad (14)$$

To determine the probability of infection (P, %) as a function of the exposure time (t) of susceptible people, the quanta concentration was integrated over time through the Wells–Riley equation [10] as follows:

$$P = \left(1 - e^{-IR \int_0^T n(t)dt} \right) \quad (\%) \quad (15)$$

IR is the inhalation rate of the exposed subject (which was assumed to be the inhalation rate for resting and standing averaged at $0.52 \frac{m^3}{h}$, and T is the total exposure time (h). From infection risk P, the number of susceptible people infected after the exposure time can be easily determined by multiplying P by the number of exposed individuals. To show the possible effect of different values of indoor relative humidity, the infection risk model from equation (15) is simulated for an indoor microenvironment of a classroom $(60\, m^2\, x\, 3\, m)$ with an infectious asymptomatic lecturer talking for 120 min for different ventilation rate scenarios (0.5, 2, and 6 ACH) and RH values (20%, 37%, 53%, 70%, and 83.5%) according to the values adopted from Fig. 2). The size of the room was selected so to represent an average classroom size based on the UK Department of Education "Area guidelines for mainstream schools" for classrooms intended for 30 pupils in schools [39]. Given the sparsity of data and the fact that the numbers would vary from patient to patient and depend on the onset of symptoms, no empirical correlation seems to have been established between viral concentrations and the severity of symptoms. Based on existing data [40–45], we tentatively classified the viral load into the following three categories:

a) Mild-to-moderate cases: $c_v = 10^7 \frac{RNA}{ml}$
b) Moderate-to-severe cases: $c_v = 10^9 \frac{RNA}{ml}$
c) Extremely severe cases: $c_v = 10^{11} \frac{RNA}{ml}$

3. Results and discussion

Traditional Wells-Riley models have been widely used as risk assessment prediction tools in pandemic outbreaks. However, these models have not reflected the effect of specific indoor environment parameters, such as relative humidity. A modified version of the Wells-Riley model is presented in the methodology section to include the impact of RH on the volume emission of respiratory droplets from an infected individual and its removal mechanisms of deposition by gravitational settling and inactivation by biological decay. Thus, we were able to determine and estimate the magnitude by which RH can affect the airborne transmission of SARS-CoV-2 and the reduction in the infection risk from one infected individual within public indoor spaces. In addition to the impact of RH, by using updated characteristics of the SARS-CoV-2 virus based on the estimated infection dose, theoretical calculations of the infection risk were performed for different scenarios considering the viral load in the infected individual, different size ranges of dehydrated respiratory droplets, and different ventilation rates.

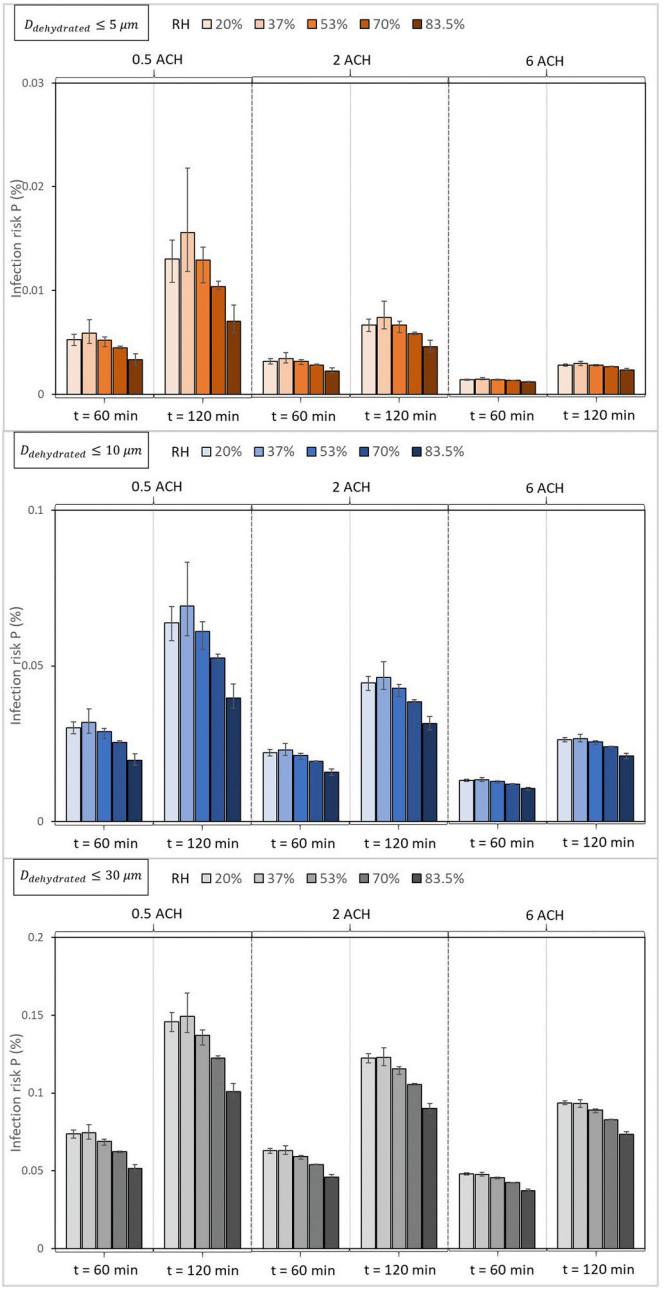

Fig. 4. Impact of RH and ventilation on infection risk P (%) when an infected person with a viral load of $c_v = 10^7 \frac{RNA}{ml}$ is speaking continuously for 60 and 120 min. The columns depict mean P (%), and the error bars present min and max values.

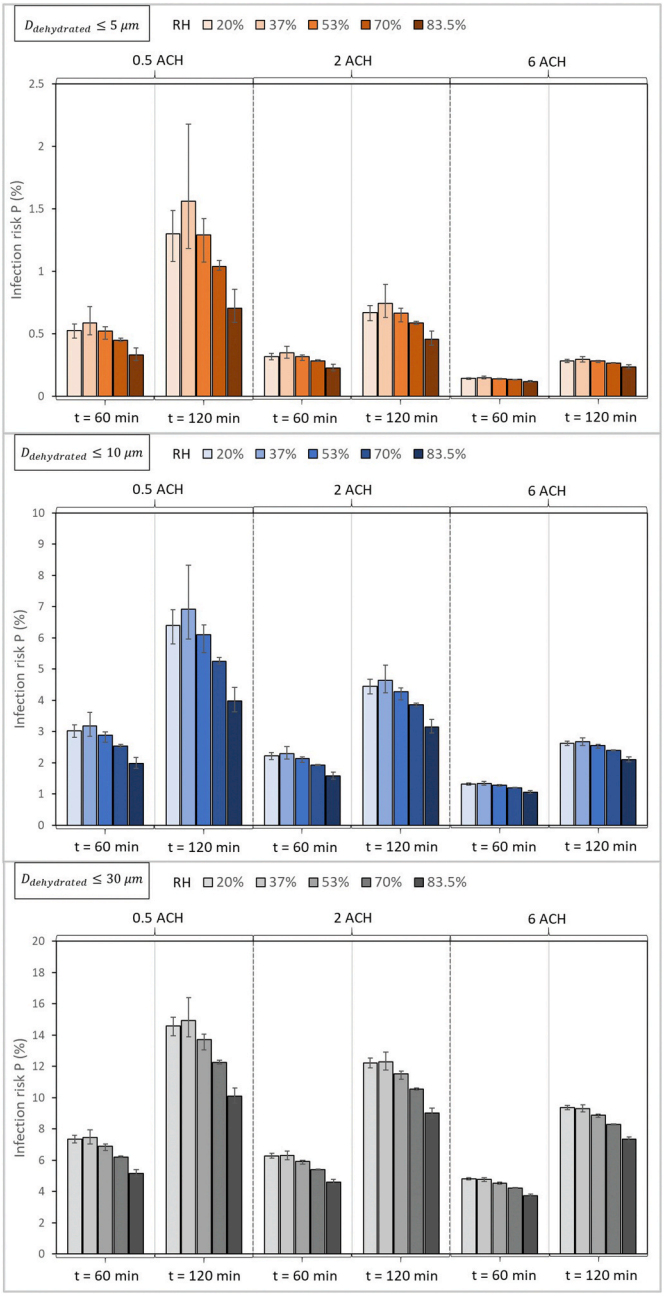

Fig. 5. Impact of RH and ventilation on infection risk P (%) when an infected person with a viral load of $c_v = 10^9 \frac{RNA}{ml}$ is speaking continuously for 60 and 120 min. The columns depict mean P (%), and the error bars present min and max values.

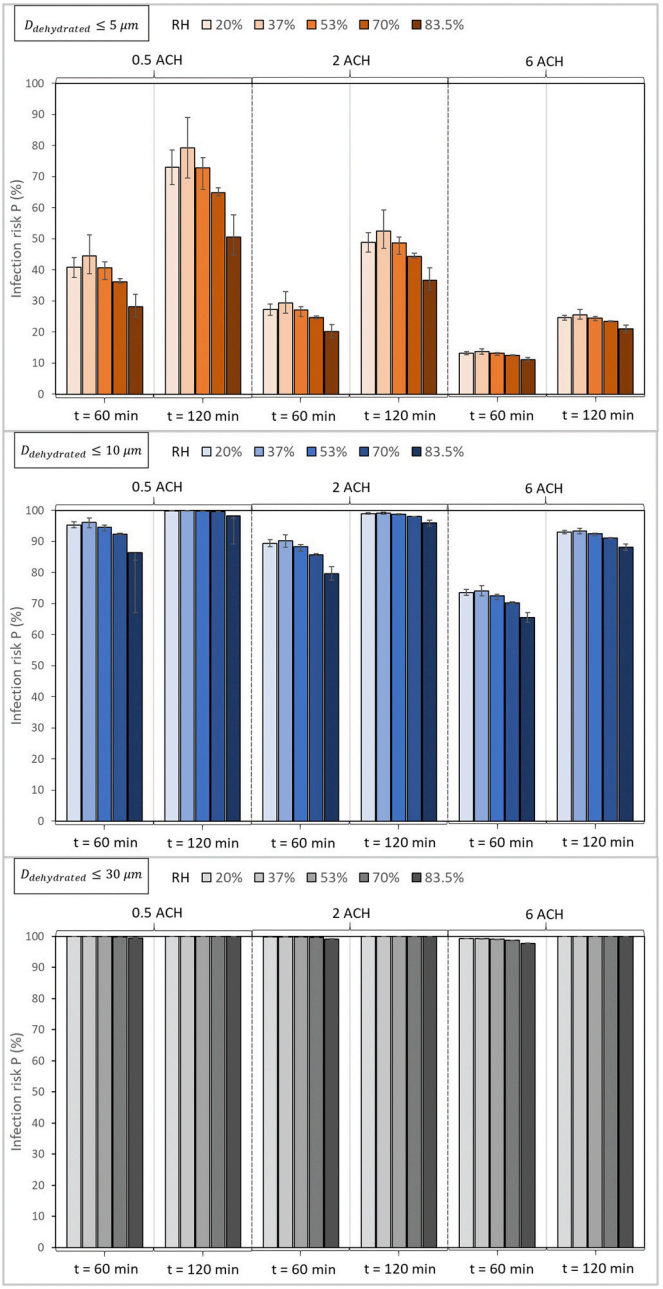

Fig. 6. Impact of RH and ventilation on infection risk P (%) when an infected person with a viral load of $c_v = 10^{11} \frac{RNA}{ml}$ is speaking continuously for 60 and 120 min. The columns depict mean P (%), and the error bars present min and max values.

3.1. The impact of RH on infection risk dynamics when an infected person is speaking

Figs. 4–6 compare the relative effect of RH for different size ranges of dehydrated respiratory droplets and various ventilation rates with outdoor air on the risk of infection caused by an infected individual carrying a viral load of $10^7 \frac{RNA}{ml}$ (Fig. 4), $10^9 \frac{RNA}{ml}$ (Fig. 5) and $10^{11} \frac{RNA}{ml}$ (Fig. 6) after continuously speaking for 120 min in a 180 m^3 room. The size range of the dehydrated respiratory droplets was classified according to the average sedimentation time [31] for the respiratory droplet to reach the ground from a height of 1.5 m: $\tau_{sed} > 60$ min for $D_{dehyd} \leq 5\ \mu m$, $\tau_{sed} > 5$ min for $D_{dehyd} \leq 10\ \mu m$ and $\tau_{sed} > 0.5$ min for $D_{dehyd} \leq 30\ \mu m$. The calculation can be interpreted as cumulative for both the quanta $n(t)$ and infection risk P (%) when considering the addition of the next successive size bin to the sum of all previous droplet size ranges. However, as the considered three size ranges $D_{dehyd} \leq 5\ \mu m$, $D_{dehyd} \leq 10$ and $D_{dehyd} \leq 30\ \mu m\ \mu m$ in our study are not successive size ranges, the results in the plots 3–5 should not be interpreted as cumulative, i.e. $P(\leq 5\ \mu m) + P(\leq 10\ \mu m) \neq P(\leq 30\ \mu m)$.

Infection risk P (%) will decrease with an increase in RH from 37% to 83.5%, particularly for RH > 53%, given the same ventilation rate, droplet size range, and viral load considered. For smaller droplets considered ($D_{dehyd} \leq 5\ \mu m$), the mean infection risks for 20% and 53% are approximately equal. As the considered droplet size ranges increase to $D_{dehyd} \leq 10\ \mu m$ and $D_{dehyd} \leq 30\ \mu m$, the mean infection risk at 20% will increase compared to that at 53%, eventually surpassing it. This happens due to the enhanced removal mechanism by gravitational settling (Figs. 7–9) with the increase in droplet size considered. Another consequence of the increased effect of gravitational settling with an increase in droplet size considered will be the decreased gaps between mean infection risks from RH = 37% to RH = 83.5%, thus minimizing the relative effect of RH on infection risk. In addition, with the increase in the size of droplets, the relative effect of ventilation on decreasing infection risk will decrease. As the exposure time passes, the dynamics of the impact of RH on infection risk will depend on the size range considered, ventilation rate, and viral load. As shown in Figs. 4–6, the difference in infection risk for different RH values will increase with exposure time at a constant ventilation rate. For higher ventilation rates, the differences between the infection risks at different RH values become relatively small, and RH will have only a minor effect if any. However, this will not be the case for lower viral loads $c_v = 10^7 \frac{RNA}{ml}$ and $c_v = 10^9 \frac{RNA}{ml}$, where the infection risk will be lower for lower ventilation rates regardless of RH values. Generally, increasing the ventilation rate will have a stronger effect in reducing infection compared to changing the relative humidity given the same exposure time and viral load considered. Changing RH in the range between 20% and 53% is ineffective, plausibly due to the nonlinearity of the relationship between RH and inactivation rates (Fig. 2). It may also be worth observing, from Fig. 6, that at very high viral loads, the relative impact of ventilation for the considered range of 0.5–6 ACH may be ineffective for larger droplets considered ($D_{dehyd} \leq 30\ \mu m$).

3.2. The impact of RH on the removal efficiency of the infectious quanta concentration after the infectious person leaves the room

The impact of RH on the removal efficiency of the infectious quanta concentration $n\,(t)$ once the infected person is absent is defined according to the following expression:

$$Removal\ efficiency = \frac{n(t + 10\ \text{min}) - n(t)}{n(t)}\,(\%)$$

where t (min) is the time step in which the person leaves the room (t = 120 min in the considered scenario).

Figs. 7–9 depict the removal efficiencies for all three mechanisms for different size ranges and ventilation rates. Regardless of the ventilation rate and droplet size considered, both the removal efficiency due to settling and inactivation increased the RH from 37% to 83.5%. The mean removal efficiency at RH = 20% will be higher than at RH = 53% for smaller droplets ($D_{dehyd} \leq 5\ \mu m$). At this size range, the differences in

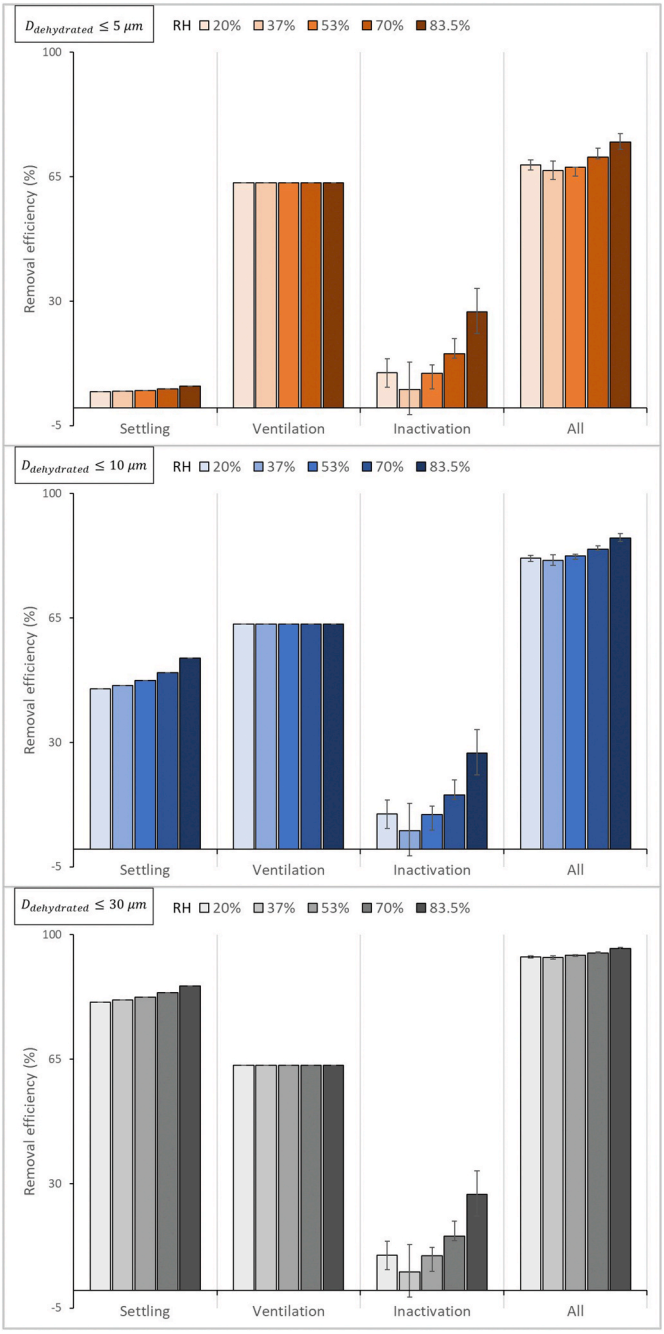

Fig. 7. Removal efficiency when individuals stopped speaking (source absent) due to gravitational settling, ventilation (set to 6 ACH), and inactivation for different size ranges of dehydrated respiratory droplets at different RHs. The columns depict the mean *Removal efficiency*, and the error bars present min and max values.

inactivation rates for different RH values will determine the overall impact of RH on removal efficiency, as removal efficiency for ventilation is not influenced by RH, while the differences in removal efficiency for settling for different RHs are too small to impact overall removal efficiency. However, as larger droplets have greater settling velocities, at higher RHs, the equilibrium droplet size will be relatively larger and will therefore accelerate the removal mechanism. Thus, with an increase in the considered droplet size range, the relative removal efficiency effect by settling will increase. Although the difference between the settling removal efficiencies at different RHs will increase with an increase in droplet size range, these differences will have a small impact compared with the overall removal efficiency at higher ventilation rates, as the ventilation rate removal efficiency is independent of RH value.

On the other hand, the removal efficiency of inactivation due to

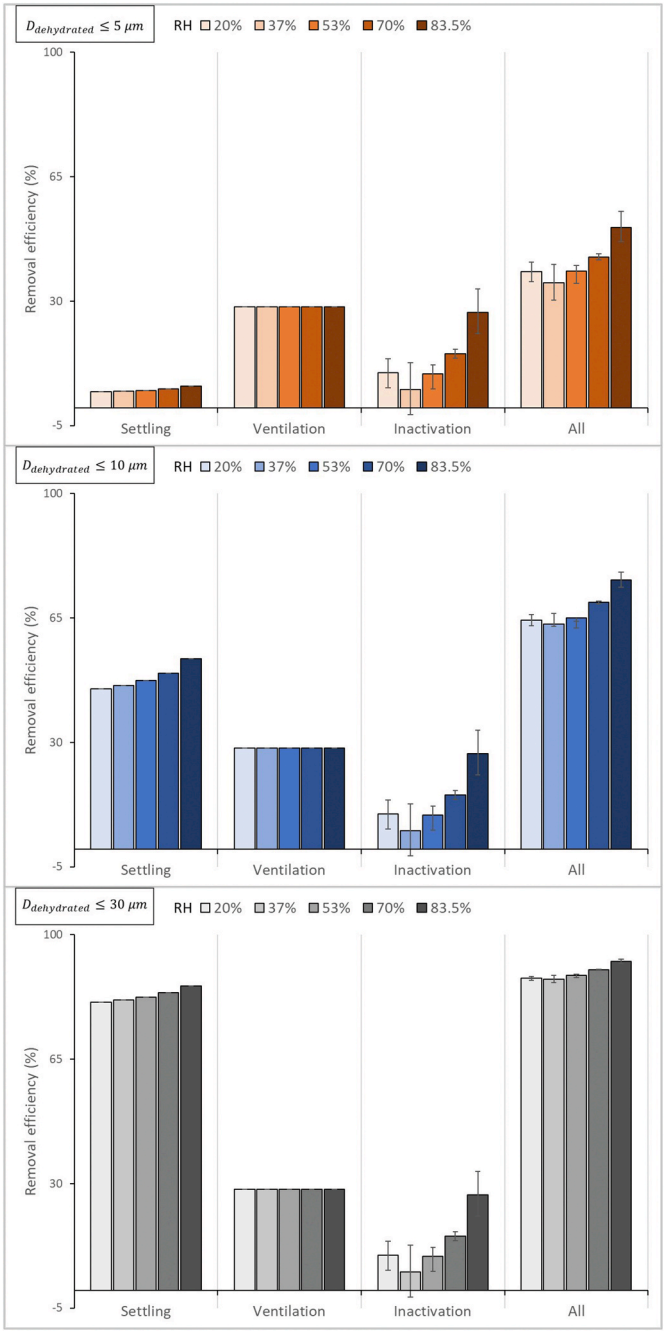

Fig. 8. Removal efficiency when individuals stopped speaking (source absent) due to gravitational settling, ventilation (set at 2 ACH), and inactivation for different size ranges of dehydrated respiratory droplets at different RHs. The columns depict the mean *Removal efficiency*, and the error bars present min and max values.

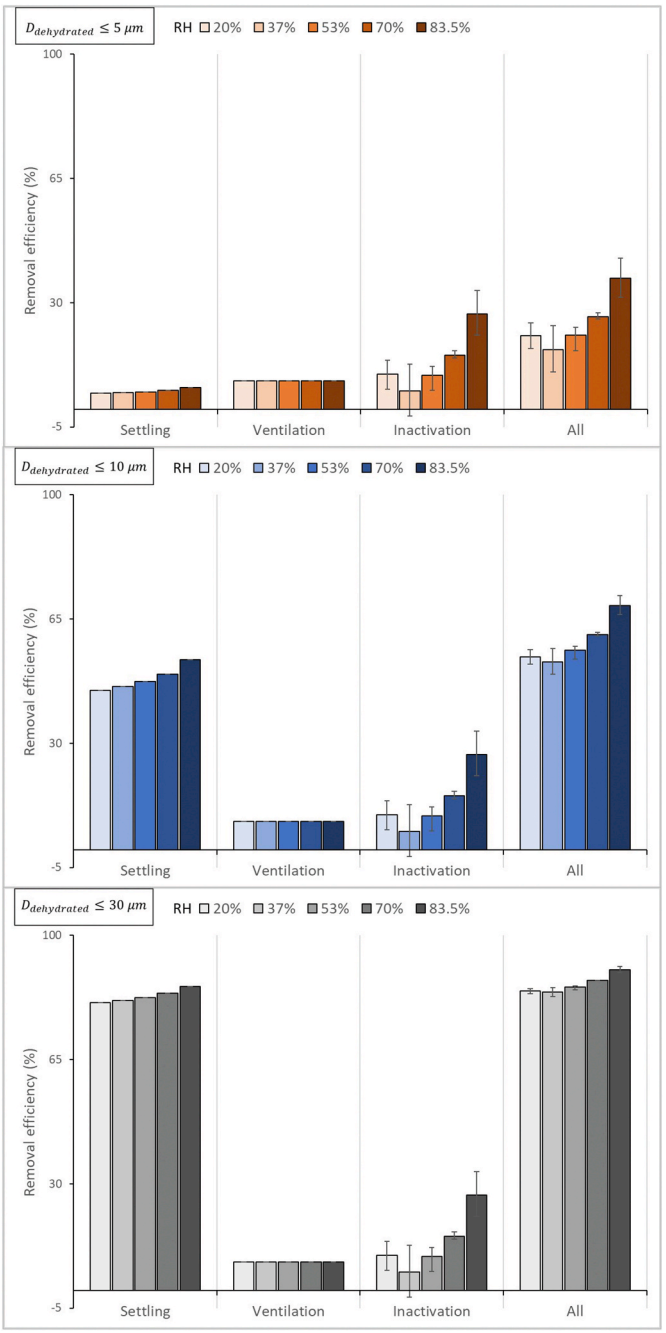

Fig. 9. Removal efficiency when individuals stopped speaking (source absent) due to gravitational settling, ventilation, and inactivation for different size ranges of dehydrated respiratory droplets at different RHs at 0.5 ACH. The columns depict the mean *Removal efficiency*, and the error bars present min and max values.

biological decay is independent of size range but is considerably affected by RH: the mean removal mechanism by biological decay at RH = 83.5% is almost three times as effective as at RH = 37%. However, the mean removal efficiencies for inactivation should be interpreted with caution due to the wide range of reported inactivation rates in the literature, specifically RH = 37% (Table 2).

The relative impact of RH will be more significant at lower ventilation rates, and the difference between the mean total removal efficiency at 20% and 83.5% RH for 6 ACHs will be approximate ~6% (Fig. 7), while the same relative difference will be close to 17% for 0.5 ACH for smaller droplets $D_{dehyd} \leq 5$ (Fig. 9). The relative impact of RH will also decrease for larger size ranges considered $D_{dehyd} \leq 10\ \mu m$ and $D_{dehyd} \leq 30\ \mu m$ due to the relative increase in the removal efficiency by gravitational settling. The relatively larger increase in removal efficiency by settling at RH = 83.5% compared to the increase in the removal efficiency at RH = 20–70% is due to the exponential increment in the size of the dehydrated respiratory droplet diameter for RH values > 65% following the separate solute volume additivity (SS-VA) model for multicomponent particles by Mikhailov et al. [25], as used in equation (12).

Ventilation can remove all droplets regardless of size but this will strongly depend on the ACH in a room. Ventilation can remove up to 60% of the droplets for higher ventilation rates (6 ACH), while the removal efficiency is less than 30% for lower ventilation rates set at 2 ACH and even less than 10% at 0.5 ACH. As the ventilation rate decreases to 2 ACH, it will no longer be the dominant removal mechanism, and together with a very low deposition rate (<10%), the overall removal efficiency will be reduced, as shown in Fig. 8. Fig. 9 also shows an increase in the difference between the overall removal efficiency rates for different values of RH at 0.5 ACH for $D_{dehyd} \leq 5\ \mu m$ compared to the same size range when 6 ACH. The relative change in the ventilation rate from 0.5 to 6 ACH has a more significant impact on increasing the total removal efficiency compared to increasing RH from 37 to 83.5%. At 6 ACH, ventilation will be the dominant removal mechanism of both respiratory droplets $D_{dehyd} \leq 5\ \mu m$ and $D_{dehyd} \leq 10\ \mu m$ but not for $D_{dehyd} \leq 30\ \mu m$, for which the settling mechanism will prevail as dominant. For dehydrated droplets $\leq 10\ \mu m$, the removal efficiency of settling increases to >40%, while for dehydrated droplets $\leq 30\ \mu m$, gravitational settling is the dominant removal efficiency, removing up to more than 80% of the droplets.

When a larger size range of droplets is considered, gravitational settling removes a large fraction of SARS-CoV-2, up to >94% for those with $D_{dehyd} \leq 30\ \mu m$ and up to 50.35% for those with $D_{dehyd} \leq 10\ \mu m$. Because settling velocity scales are proportional to diameter squared, removal efficiencies due to gravitational settling range from only 4.5–5.7% for $D_{dehyd} \leq 5\ \mu m$. This rather low removal inefficiency by settling can be compensated by a higher ACH in a room, and the removal efficiency by ventilation can be lower than 10% for a small ventilation rate (0.5 ACH) and >60% for a higher ventilation rate (6 ACH). Figs. 7–9 also show that removal by inactivation is more variable in association with RH than removal by gravitational settling. This finding implies that for very low ventilation rates, controlling indoor RH may play an important role as a removal mechanism (inactivation) for small airborne infectious droplets (≤5 μm). However, as Fig. 10 shows, maintaining a higher ventilation rate will have a more beneficial effect on the removal of airborne SARS-COV-2 compared to only increasing RH for small airborne infectious droplets (≤5 μm). Generally, higher ventilation rates and a higher RH will result in the highest total removal efficiency, regardless of the droplet size considered.

3.3. Comparison with other contemporary studies using modified versions of the Wells-Riley model

Overall, for the considered exposure time of 60 min, at a ventilation rate of 6 ACH and RH = 83.5%, the lowest infection risk was P = 0.0033% (Fig. 4) caused by small respiratory droplets ($D_{dehyd} \leq 5\ \mu m$) carrying a viral load concentration of $10^7\ \frac{RNA}{ml}$. The maximum infection risk of 99.99% was reached for larger respiratory droplets ($D_{dehyd} \leq 30\ \mu m$) carrying a viral load concentration of $10^{11}\ \frac{RNA}{ml}$ at RH = 37.5% and at a ventilation rate of 0.5 ACH. The latter maximum infection risk

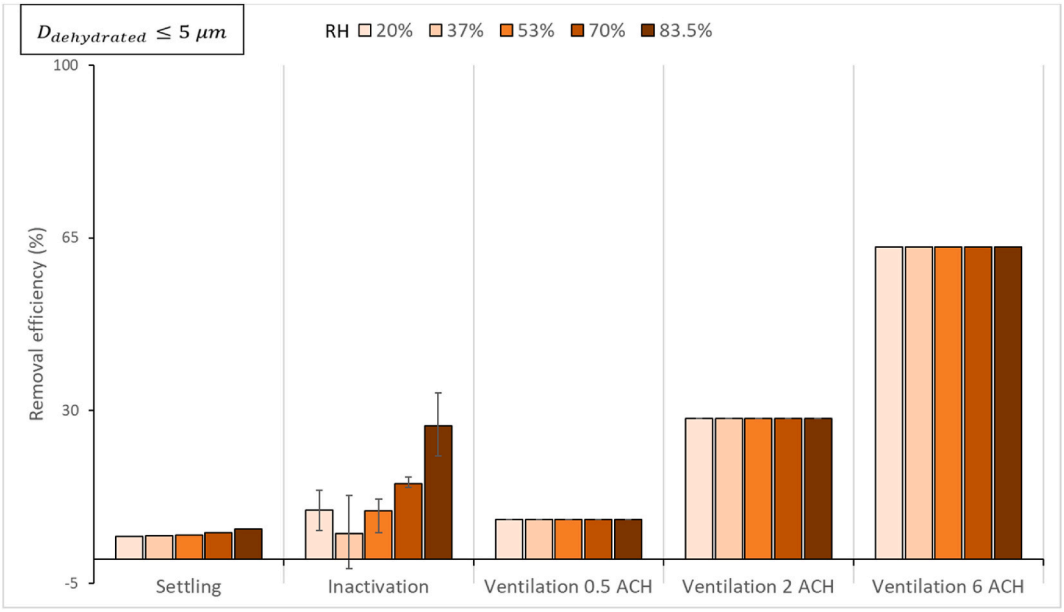

Fig. 10. Removal efficiency when individuals stopped speaking (source absent) due to gravitational settling, inactivation, and three different ventilation rates (0.5, 2, and 6 ACH) for small airborne infectious droplets (≤5 μm). The columns depict the mean *Removal efficiency*, and the error bars present min and max values.

Table 2
Data from previous studies using modified Wells-Riley models to evaluate the infection risk from SARS-COV-2 in well-mixed indoor spaces.

Study	Droplet size range	Droplet volume concentration $\left(\frac{ml}{h}\right)$	$c_i = \left(\frac{quanta}{RNA}\right)$	$c_v = \left(\frac{RNA}{ml}\right)$	Inhalation rate $IR\left(\frac{m^3}{h}\right)$	Room Volume (m^3)	ACH	Emission time (min)	Infection risk $P(\%)$ in original study	Infection risk[a] $P(\%)$ according to eq. (15) $D_{dehyd} \leq 5\mu m$	Infection risk[a] $P(\%)$according to eq. (15) $D_{dehyd} \leq 20$ µm
Buoannano et al. [16]	$D_{hyd} \leq 5.5$ µm	$4.41{\cdot}10^{-7}$	$2{\cdot}10^{-2}$	10^9	0.96	75	2.2	10	~4	0.15–0.16	–
Buoannano et al. [47]	$D_{dehyd} \sim 4$ µm	$3{\cdot}10^{-2}$	$3.66{\cdot}10^{-5}$	10^7	1.38	800	0.5	120	2.1	0.01–0.03	–
De Oliveira et al. [49]	$D_{dehyd} \leq 5$µm	–	$2.43{\cdot}10^{-3}$	10^9	1.87	200	5	60	0.5	1.54–2.01	–
Schijven et al. [32] [b]	$D_{dehyd} \leq 20$ µm	$0.77–1.08{\cdot}10^{-6}$	$6.94{\cdot}10^{-4}$	10^7	0.94–1.16	100	0	20	<0.01	–	0.06–0.08
							6	120	$0.1 < P < 0.01$	–	0.41–0.53
Current Study	$D_{dehyd} \leq 5$µm	$8.66{\cdot}10^{-6}$	$6.94{\cdot}10^{-4}$	10^7–10^{11}	0.54	180	0.5–6	45	Infection risk P (%) values shown in Figs. 3–5		
	$D_{dehyd} \leq 10$ µm	$1.28{\cdot}10^{-4}$									
	$D_{dehyd} \leq 30$ µm	$1.06{\cdot}10^{-3}$									

[a] Probability infection P (%) was calculated according to equation (17) for the same values of the input parameters inhalation rate IR, ACH, room volume, emission time, and c_v as in the original study.
[b] Inhalation rate was used instead of deposition as a removal mechanism.

scenario at t = 60 min may not be as realistic as it is based on droplets with an insufficient airborne survival time scale compared to the air-change time scale. Therefore, a more realistic maximum infection risk would be P = 96.0% at RH = 37.5% for the same amount of viral load but for respiratory droplets with a sedimentation time of at least 5 min ($D_{dehyd} \leq 10\ \mu m$). It is also clear from Figs. 4–6 that the viral load has a major impact on whether the infection risk is large enough to be considered significant (>0.1%): the maximum infection risk for $D_{dehyd} \leq 10\ \mu m$for a viral load of $10^7\ \frac{RNA}{ml}$ instead of $10^{11}\ \frac{RNA}{ml}$ would drop from P = 96.0% to as low as 0.03%. Again, the latter scenario may be more realistic, as several analyses of the viral load of SARS-COV-2 in clinical samples have indicated a mean load in the range of 10^5-$10^6\ \frac{RNA}{ml}$ [40–42], while the maximum reported load of $1.34{\cdot}10^{11}\ \frac{RNA}{ml}$ was identified as a highly symptomatic person who later died [41]. Nevertheless, several studies of SARS-CoV-2-infected individuals have demonstrated asymptomatic cases to have a viral load as high as in symptomatic patients [43,44]: viral loads as high as $10^9\ \frac{RNA}{ml}$ have been reported in the sputum of asymptomatic persons [45]. In this context, it is important to compare the results from this study with other studies using modified versions of the Wells-Riley model to simulate infection risks for scenarios when an infected person talks in a well-mixed indoor space. For an absolute comparison, the infection risk P (%) in equation (15) was calculated for the same values of input parameters inhalation rate IR, ACH, room volume, emission time, and c_v as in the original studies considered (Table 2).

Among the first assessment studies on the infection risk of airborne transmission of SARS-COV-2 using Wells-Riley, Buonanno et al. [16] simulated the infection risk to be 3.5–4% after an infected person with a viral load of $10^9\ \frac{RNA}{ml}$ was speaking for 10 min in a 75 m^3-size pharmacy. This infection risk is approximately 30 times higher than the infection risk caused by the same viral load after 10 min simulated by our model, considering the same respiratory droplet size range considered at $\leq 5\ \mu m$. This significant difference is due to the difference between the values used to describe the conversion factor for the dose-response relationship $c_i$between one quantum and the amount of virus needed to infect at least 63.2% of the susceptible population, where Buonanno et al. used $c_i = 2{\cdot}10^{-2}\ \frac{quanta}{RNA}$ for SARS-COV-1. Although a dose-response relationship c_i for SARS-COV-2 has not yet been found, we used the same estimation that Schijven et al. [32] used most recently, based on the fraction of RNA virus copies that were able to infect a single cell of Dutch SARS-CoV-2 isolate and the dose-response data for human coronavirus 229E (as recommended by Haas [44] to be used for SARS-COV-2). This value was approximately 30 times lower than the value used by Buonanno et al. [16], thus it may explain the calculated differences.

Although a much lower conversion factor c_i value was used in a later assessment risk study by the same group of authors [46] for a loud-speaking infected person in an 800 m^3-size auditorium, the infection risk after 120 min for a viral load of $10^7\ \frac{RNA}{ml}$ was at least 320 times the infection risk calculated by our model, given the same input parameters of inhalation rate IR, ACH, and size range of respiratory droplets. The significant difference used to estimate the volume concentration of respiratory droplets expelled from a speaking person $\left(\frac{ml}{h}\right)$is the reason for this finding. In the study mentioned, Buonanno et al. [47] referred to the estimated volume emitted by a loud-speaking person provided by Stadnytskyi et al. [48], considering droplet dehydration. However, the dehydrated volume droplet from Stadnytskyi et al. [48] of $\sim 3.17{\cdot}10^{-4}\ \frac{ml}{h}$ has been misreported as $3{\cdot}10^{-2}\ \frac{ml}{h}$, consequently resulting in very large infection risks.

In a recent study, De Oliveira et al. [49] obtained a lower infection risk, around P = 0.5%, after 60 min of an infected person speaking, which is approximately 2–3 times lower than our results for the same dehydrated droplet range considered ($\leq 5\mu m$) for the same viral load $10^9\ \frac{RNA}{ml}$ and the same ACH. The main difference in the approach used by

De Oliveira et al. [49] is that they calculated the initial number of virus copies based on the volume of dehydrated droplets and not the volume of the original sizes of the respiratory droplets as used in our assumption. The initial size of a hydrated respiratory droplet (emitted 99.5% RH) can be 2–3 times larger than the dehydrated equilibrium droplet, depending on the RH value, which will have a significant effect on the total calculated volume of the droplets and consequently on the initial amount of viral RNA copies. The reason why we assumed that the initial amount of virus copies is proportional to the initial volume size of hydrated droplets is that there is simply no evidence showing that the inactivation/destruction of the virus content in droplets is proportional to the shrinkage in volume size within only several seconds of the evaporation process. Rather, this inactivation process of the initial amount of viral content present in hydrated droplets during the evaporation process is taken into account due to biological decay (Fig. 2). In addition, De Oliveira et al. [49] used a 3.5 times lower c_i value (based on data for SARS-COV-1). This difference was more than compensated for by the difference in the different droplet volumes estimated: the one in Ref. [49] is calculated by the trimodal lognormal distribution (BLO) provided by Johnson et al. [50], while our model is based on representative droplet diameters from size bins as measured by Morawska et al. [17] for droplet aerosols $\leq 2\ \mu m$ and Chao et al. [35] for respiratory droplets $\geq 2\ \mu m$. It is very difficult from this standpoint to interpret which method is more accurate, as previous methods measuring the size distributions derived by droplet dispersal from a speaking person have been shown to be lower than the BLO model for droplets $\leq 5\ \mu m$ in size [50].

Finally, we also compared the results from our study to the recent results that Schijven et al. obtained [32] for $D_{dehyd} \leq 20\ \mu m$ using the same conversion factor c_i, when using the same input value in our model for a 120-min scenario with 6 ACHs for a viral load of $c_i = 10^7\ \frac{RNA}{ml}$. Again, the reason is the same as for De Oliveira et al. [48]: The initial number of virus copies (RNA) was calculated based on the dehydrated droplet volume concentration immediately after evaporation and not the original size of the respiratory droplets at the mouth opening. However, one must be cautious when interpreting the results from Ref. [32], as it did not consider the removal mechanism by deposition but instead inhalation. The overall comparison with previous studies emphasizes the sensitivity of infection risk calculations by Wells-Riley models to input parameters that are very difficult to standardize due to their peculiarity, i.e., the droplet volume concentration expelled from an infected person and the viral load, but primarily the dose-response conversion factor c_i, which may be subject to continuous change due to the new variants of the virus that are emerging.

The lack of a standardized value or calculation method for respiratory droplet volume emission from infected persons may result in significant deviations in the infection risk calculated by similar versions of the modified Wells-Riley model, resulting in inconsistent results for the same case scenarios in different studies. Consequently, the different outcomes calculated by open-access computational tools based on such studies for the same scenarios may incite not only misleading guidelines by public health authorities but also general confusion in public opinion about the infection risk in enclosed spaces. The results of this study may support public health authorities in reconsidering engineering measures for infection control.

3.4. Model limitations

There are several limitations of our model. The assumption that expelled aerosol droplets are evenly distributed in the air of the room implies that there is an immediate dilution of the expelled virus concentration. In reality, dilution does not occur instantaneously; it is highly dependent on the movement of the air in the room. Even in a well-mixed room, an exposed person standing directly in front of the infected person may inhale a much larger dose of airborne particles than an exposed person physically distanced by at least 1 m. Another limitation of the present work is that the Wells-Riley model can simulate only complete mixing within a space. Novel and advanced ventilation systems with the same ventilation rates as traditional systems have been shown to have higher ventilation efficiencies, i.e., better dilution was obtained [51]. Consequently, the present results are valid only when complete mixing is obtained. The assumption that the expelled aerosol droplets are evenly distributed in the room air implies an immediate dilution of the expelled virus concentration, which is relatively rare. This is yet another limitation of the present work. In-situ validation of the present results would be helpful but is challenging to execute.

The droplet size distribution expelled from a human respiratory tract used was derived from studies on healthy persons, which may differ from the volume distribution exhaled from symptomatic individuals. First, although the model used to impact RH on droplet sizes due to hygroscopic growth has been confirmed with experiments using NaCl-bovine serum albumin particles [37], further validation with actual respiratory mucus is needed due to its complex composition. Furthermore, the composition of respiratory fluid depends on the emission site (nose or mouth) and source (upper or lower respiratory tract) as well as the stage of the infection. Inflamed airways excrete larger amounts of mucus, which may increase the dry mass portion of respiratory fluid [52] and thus may misrepresent the equilibrium size of emitted droplets calculated in this paper that was based on composition under healthy conditions. Another possible limitation is that the resuspension effect has been excluded as a removal mechanism in our version of the Wells-Riley model, as previous studies on the airborne transmission of respiratory diseases have shown that disease transmission could depend on the resuspension of floor dust [53]. This model does not consider the possible impact of different chemical compositions of the droplets on virus viability, i.e., the protein, salt, and surfactant concentrations [54]. The evaluation of the infection risk does not consider the human immune system's reaction to changes in RH. It should also be noted that the values calculated with this model could vary significantly as a function of the activity levels of both the infected subject and the viral load in the sputum of the infected subject. It was also assumed that the infected individual was talking constantly, which may present an unrealistic overproduction of the number of respiratory droplets expelled. In addition, as may be observed from Table 2, the probability of infection calculated according to equation (15) is strongly dependent on the dose-response relationship c_i. To allow for a more absolute comparison between infection risks from different studies, other assessment methods, which are independent of the dose-response data [55,56], should be used in future studies. We did not examine the effect of room size as this was not our objective. Further data on this issue can be found in other publications, e.g. Ref. [57]. The current model is limited to five RH levels based on the data from three different studies investigating SARS-CoV-2 inactivation rates; the data for one temperature of $T = 20°C$ was used as typical indoors. Consequently, the trends and accuracy of the numeric estimates presented in the present paper should be interpreted with caution at other temperature levels, especially lower than 20 °C and higher than 25 °C. The temperature change between 20 and 25 °C was not found to have a significant effect on dehydrated droplet diameter.

4. Conclusions

The infection risk was calculated using the modified Wells-Riley model at five different RH levels: 20%, 37%, 53%, 70%, and 83.5% for a specific indoor scenario when an infected person was continuously talking for 120 min. 70% and 83.5% represent extremely high humidity levels not relevant for indoor spaces but were included for comparative purposes.

The findings of the study can be summarized in the following key points:

- The impact of RH on infection risk was found to be dependent on the ventilation rate and the size range of droplets.
- Within the RH range of 20%–53%, typical of indoor spaces in temperate and cold climates, the highest mean and maximum infection risk was always seen at an RH of 37%, while it was lower at RHs of 20% and 53%, regardless of the droplet size and ventilation rate.
- Increasing RH from 37% to 53% was shown to reduce the mean infection rate by no more than 7% for the same size range of droplets ($D_{dehyd} \leq 5\ \mu m$) at a ventilation rate of 0.5 ACH. The same increase in RH at 6 ACH was shown to reduce the infection rate by no more than 1%.
- Increasing the ventilation rate from 0.5 ACH to 6 ACH was shown to decrease the infection risk by up to 54% at a constant RH for droplet size $D_{dehyd} \leq 5\ \mu m$.
- Ventilation was shown to be the dominant removal mechanism of small infectious respiratory droplets ($D_{dehyd} \leq 5\ \mu m$) that may remain suspended in the air over long distances and during long periods. A significant impact on the removal of larger droplets ($D_{dehyd} \leq 10\ \mu m$ and $D_{dehyd} \leq 30\ \mu m$) was also observed.

In conclusion, we showed that maintaining a higher ventilation rate had a more beneficial effect on the removal of airborne SARS-CoV-2 than changing RH. These results emphasize the key role of ventilation in controlling the virus concentration in the air. Our results show that humidification to a moderate RH of 40%–60%, which is possible in many indoor spaces, is not a sufficiently effective solution for the infection risk control of SARS-CoV-2, considering the removal of droplets by gravitational setting and the biological decay of virus in the droplets. The effect of RH on the susceptibility to the SARS-CoV-2 virus was not considered and should be investigated in future experiments.

Declaration of competing interest

The authors declare that they have no known competing financial interests or personal relationships that could have appeared to influence the work reported in this paper.

Acknowledgments

This research was supported by the Estonian Research Council (grant No. COVSG38).

Appendix A. Supplementary data

Supplementary data to this article can be found online at https://doi.org/10.1016/j.buildenv.2021.108278.

References

[1] World Health Organization, Transmission of SARS-CoV-2: Implications for Infection Prevention Precautions: Scientific Brief, 09 July 2020, World Health Organization, 2020.
[2] L. Morawska, D.K. Milton, It is time to address airborne transmission of coronavirus disease 2019 (COVID-19), Clin. Infect. Dis. 71 (9) (2020 Dec 3) 2311–2313, https://doi.org/10.1093/cid/ciaa939. PMID: 32628269; PMCID: PMC7454469.
[3] L. Morawska, J. Cao, Airborne transmission of SARS-CoV-2: the world should face the reality, Environ. Int. 139 (2020 Jun) 105730, https://doi.org/10.1016/j.envint.2020.105730. Epub 2020 Apr 10. PMID: 32294574; PMCID: PMC7151430.
[4] N. Wilson, S. Corbett, E. Tovey, Airborne transmission of covid-19, BMJ 370 (2020), m3206, https://doi.org/10.1136/bmj.m3206_pmid:3281996.
[5] L. Setti, F. Passarini, G. De Gennaro, P. Barbieri, M.G. Perrone, M. Borelli, J. Palmisani, A. Di Gilio, P. Piscitelli, A. Miani, Airborne transmission route of COVID-19: why 2 meters/6 feet of inter-personal distance could not Be enough, Int. J. Environ. Res. Publ. Health 17 (8) (2020 Apr 23) 2932, https://doi.org/10.3390/ijerph17082932.PMID:32340347. PMCID: PMC7215485.
[6] R. Zhang, Y. Li, A.L. Zhang, Y. Wang, M.J. Molina, Identifying airborne transmission as the dominant route for the spread of COVID-19, Proc. Natl. Acad. Sci. Unit. States Am. 117 (26) (2020) 202009637.
[7] K. Nissen, et al., Long-distance airborne dispersal of SARS-CoV-2 in COVID-19 wards, Sci. Rep. 10 (2020) 19589.
[8] L. Liu, J. Wei, Y. Li, A. Ooi, Evaporation and dispersion of respiratory droplets from coughing, Indoor Air 7 (1) (2017) 179–190. PMID: 26945674, 10.1111/ina.12297.
[9] C.H. Cheng, C.L. Chow, W.K. Chow, Trajectories of large respiratory droplets in indoor environment: a simplified approach, Build. Environ 183 (2020).
[10] J.W. Tang, W.P. Bahnfleth, P.M. Bluyssen, G. Buonanno, J.L. Jimenez, J. Kurnitski, Y. Li, S. Miller, C. Sekhar, L. Morawska, L.C. Marr, A.K. Melikov, W.W. Nazaroff, P. V. Nielsen, R. Tellier, P. Wargocki, S.J. Dancer, Dismantling myths on the airborne transmission of severe acute respiratory syndrome coronavirus-2 (SARS-CoV-2), J. Hosp. Infect. 110 (2021 Apr) 89–96, https://doi.org/10.1016/j.jhin.2020.12.022. Epub 2021 Jan 13. PMID: 33453351; PMCID: PMC7805396.
[11] E.C. Riley, G. Murphy, R.L. Riley, Airborne spread of measles in a suburban elementary school, Am. J. Epidemiol. 107 (1978) 421–432.
[12] W.F. Wells, Airborne Contagion and Air Hygiene, Cambridge University Press, Cambridge MA, 1955, pp. 117–122.
[13] C.B. Beggs, C.J. Noakes, P.A. Sleigh, L.A. Fletcher, K. Siddiqi, The transmission of tuberculosis in confined spaces: an analytical study of alternative epidemiological models, Int. J. Tubercul. Lung Dis. 7 (2003) 1015–1026.
[14] L. Gammaitoni, M.C. Nucci, Using a mathematical model to evaluate the efficacy of TB control measures, Emerg. Infect. Dis. 3 (1997) 335–342, https://doi.org/10.3201/eid0303.970310.
[15] G.N. Sze To, C.Y. Chao, Review and comparison between the Wells-Riley and dose-response approaches to risk assessment of infectious respiratory diseases, Indoor Air 20 (1) (2010 Feb) 2–16, https://doi.org/10.1111/j.1600-0668.2009.00621.x. Epub 2009 Jul 31. PMID: 19874402; PMCID: PMC7202094.
[16] G. Buonanno, L. Stabile, L. Morawska, Estimation of airborne viral emission: quanta emission rate of SARS-CoV-2 for infection risk assessment, Environ. Int. 141 (2020) 105794, https://doi.org/10.1016/j.envint.2020.105794.
[17] L. Morawska, G.R. Johnson, Z.D. Ristovski, M. Hargreaves, K. Mengersen, S. Corbett, C.Y.H. Chao, Y. Li, D. Katoshevski, Size distribution and sites of origin of droplets expelled from the human respiratory tract during expiratory activities, J. Aerosol Sci. 40 (2009) 256–269, https://doi.org/10.1016/j.jaerosci.2008.11.002.
[18] A. Božič, M. Kanduč, Relative humidity in droplet and airborne transmission of disease, J. Biol. Phys. 47 (2021) 1–29, https://doi.org/10.1007/s10867-020-09562-5.
[19] P.G. da Silva, M.S.J. Nascimento, R.R.G. Soares, S.I.V. Sousa, J.R. Mesquita, Airborne spread of infectious SARS-CoV-2: moving forward using lessons from SARS-CoV and MERS-CoV, Sci. Total Environ. 764 (2021 Apr 10) 142802, https://doi.org/10.1016/j.scitotenv.2020.142802. Epub 2020 Oct 8. PMID: 33071145; PMCID: PMC7543729.
[20] P. Mecenas, R. Bastos, A.C.R. Vallinoto, D. Normando, Effects of temperature and humidity on the spread of COVID-19: a systematic review, PloS One 15 (9) (2020), e0238339. PubMed PMID: 32946453. PMCID: PMC7500589. Epub 2020/09/19).
[21] A. Tobías, T. Molina, M. Rodrigo, M. Saez, Meteorological factors and incidence of COVID-19 during the first wave of the pandemic in Catalonia (Spain): a multi-county study, One Health 12 (2021 Jun) 100239, https://doi.org/10.1016/j.onehlt.2021.100239. Epub 2021 Mar 29. PMID: 33816746; PMCID: PMC8007195.
[22] J. Yuan, Y. Wu, W. Jing, et al., Association between meteorological factors and daily new cases of COVID-19 in 188 countries: a time series analysis, Sci. Total Environ. 780 (2021) 146538, https://doi.org/10.1016/j.scitotenv.2021.146538.
[23] P. Dabisch, M. Schuit, A. Herzog, K. Beck, S. Wood, M. Krause, D. Miller, W. Weaver, D. Freeburger, I. Hooper, The influence of temperature, humidity, and simulated sunlight on the infectivity of SARS-CoV-2 in aerosols, Aerosol. Sci. Technol. 55 (2) (2020) 1–15.
[24] M. Schuit, S. Ratnesar-Shumate, J. Yolitz, G. Williams, W. Weaver, B. Green, D. Miller, M. Krause, K. Beck, S. Wood, Airborne SARS-CoV-2 is rapidly inactivated by simulated sunlight, JID (J. Infect. Dis.) 222 (4) (2020) 564–571, https://doi.org/10.1093/infdis/jiaa334.
[25] S.J. Smither, L.S. Eastaugh, J.S. Findlay, M.S. Lever, Experimental aerosol survival of SARSCoV- 2 in artificial saliva and tissue culture media at medium and high humidity, Emerg. Microb. Infect. 9 (1) (2020) 1–9.
[26] H. Köhler, The nucleus in and the growth of hygroscopic droplets, Trans. Faraday Soc. 32 (1936) 1152–1161.
[27] ANSI/ASHRAE, ANSI/ASHRAE standard 169-2013, in: Climatic Data for Building Design Standards, 8400, 2013, p. 104.
[28] CEN, EN 16798 Energy Performance of Buildings - Part 1: Indoor Environmental Input Parameters for Design and Assessment of Energy Performance of Buildings Addressing Indoor Air Quality, Thermal Environment, Lighting and Aco Ustics, 2019.
[29] Salah, et al., Nasal mucociliary transport in healthy subjects is slower when breathing dry air, Eur. Respir. J. 1 (9) (1988) 852–855.
[30] Kudo, et al., Low ambient humidity impairs barrier function and innate resistance against influenza infection, Proc. Natl. Acad. Sci. Unit. States Am. (2019) 1–6.
[31] R.R. Netz, Mechanisms of airborne infection via evaporating and sedimenting droplets produced by speaking, J. Phys. Chem. B 124 (33) (2020 Aug 20) 7093–7101, https://doi.org/10.1021/acs.jpcb.0c05229. Epub 2020 Jul 31. PMID: 32668904; PMCID: PMC7409921.
[32] J. Schijven, L.C. Vermeulen, A. Swart, A. Meijer, E. Duizer, A.M. de Roda Husman, Quantitative microbial risk assessment for airborne transmission of SARS-CoV-2 via breathing, speaking, singing, coughing, and sneezing, Environ. Health Perspect. 129 (4) (2021) 47002, https://doi.org/10.1289/EHP7886.
[33] W.C. Adams, Measurement of breathing rate and volume in routinely performed daily activities, 1993. Final Report. Human Performance Laboratory, Physical Education Department, University of California, Davis. Human Performance Laboratory, Physical Education Department, University of California, Davis.

Prepared for the California Air Resources Board, Contract No. A033-205, April 1993.
[34] M. Nicas, W.W. Nazaroff, A. Hubbard, Toward understanding the risk of secondary airborne infection: emission of respirable pathogens, J. Occup. Environ. Hyg. 2 (3) (2005 Mar) 143–154, https://doi.org/10.1080/15459620590918466.PMID: 15764538. PMCID: PMC7196697.
[35] C.Y.H. Chao, M.P. Wan, L. Morawska, G.R. Johnson, Z.D. Ristovski, M. Hargreaves, K. Mengersen, S. Corbett, Y. Li, X. Xie, D. Katoshevski, Characterization of expiration air jets and droplet size distributions immediately at the mouth opening, J. Aerosol Sci. 40 (2009) 122–133.
[36] W.R.A. Goossens, Review of the empirical correlations for the drag coefficient of rigid spheres, Powder Technol. 352 (2019) 350–359.
[37] E. Mikhailov, S. Vlasenko, R. Niessner, U. Poschl, Interaction of aerosol particles composed of protein and salts with water vapor: hygroscopic growth and microstructural rearrangement, Atmos. Chem. Phys. 4 (2004) 323–350.
[38] W. Yang, L.C. Marr, Dynamics of airborne influenza A viruses indoors and dependence on humidity, PloS One 6 (6) (2011), e21481.
[39] Building Bulletin 103 (BB103): *Area Guidelines for Mainstream Schools*, Uk Department for Education, London, United Kingdom, 2014.
[40] E. Pujadas, F. Chaudhry, R. McBride, F. Richter, S. Zhao, A. Wajnberg, G. Nadkarni, B.S. Glicksberg, J. Houldsworth, C. Cordon-Cardo, SARS-CoV-2 viral load predicts COVID-19 mortality, Lancet Respir Med. 8 (9) (2020 Sep) e70, https://doi.org/10.1016/S2213-2600(20)30354-4. Epub 2020 Aug 6. PMID: 32771081; PMCID: PMC7836878.
[41] Y. Pan, D. Zhang, P. Yang, L.L.M. Poon, Q. Wang, Viral load of SARS-CoV-2 in clinical samples, Lancet Infect. Dis. 20 (4) (2020 Apr) 411–412, https://doi.org/10.1016/S1473-3099(20)30113-4. Epub 2020 Feb 24. PMID: 32105638; PMCID: PMC7128099. Virological assessment of hospitalized patients with COVID-2019.
[42] R. Wölfel, V.M. Corman, W. Guggemos, M. Seilmaier, S. Zange, M.A. Müller, D. Niemeyer, T.C. Jones, P. Vollmar, C. Rothe, M. Hoelscher, T. Bleicker, S. Brünink, J. Schneider, R. Ehmann, K. Zwirglmaier, C. Drosten, C. Wendtner, Virological assessment of hospitalized patients with COVID-2019, Nature 581 (7809) (2020 May) 465–469, https://doi.org/10.1038/s41586-020-2196-x. Epub 2020 Apr 1. Erratum in: Nature. 2020 Dec;588(7839):E35. PMID: 32235945.
[43] L. Zou, F. Ruan, M. Huang, L. Liang, H. Huang, Z. Hong, J. Yu, M. Kang, Y. Song, J. Xia, Q. Guo, T. Song, J. He, H.L. Yen, M. Peiris, J. Wu, SARS-CoV-2 viral load in upper respiratory specimens of infected patients, N. Engl. J. Med. 382 (12) (2020 Mar 19) 1177–1179, https://doi.org/10.1056/NEJMc2001737. Epub 2020 Feb 19. PMID: 32074444; PMCID: PMC7121626.
[44] I. Hasanoglu, G. Korukluoglu, D. Asilturk, Y. Cosgun, A.K. Kalem, A.B. Altas, B. Kayaaslan, F. Eser, E.A. Kuzucu, R. Guner, Higher viral loads in asymptomatic COVID-19 patients might be the invisible part of the iceberg, Infection 49 (1) (2021 Feb) 117–126, https://doi.org/10.1007/s15010-020-01548-8. Epub 2020 Nov 24. PMID: 33231841; PMCID: PMC7685188.
[45] C. Rothe, M. Schunk, P. Sothmann, G. Bretzel, G. Froeschl, C. Wallrauch, T. Zimmer, V. Thiel, C. Janke, W. Guggemos, M. Seilmaier, C. Drosten, P. Vollmar, K. Zwirglmaier, S. Zange, R. Wölfel, M. Hoelscher, Transmission of 2019-nCoV infection from an asymptomatic contact in Germany, N. Engl. J. Med. 382 (10) (2020 Mar 5) 970–971, https://doi.org/10.1056/NEJMc2001468. Epub 2020 Jan 30. PMID: 32003551; PMCID: PMC7120970.
[46] C.N. Haas, Action levels for SARS-CoV-2 in air: a preliminary approach, OSF Preprints (2020), https://doi.org/10.31219/osf. io/erntm. Preprint posted online August 14, 2020.
[47] G. Buonanno, L. Morawska, L. Stabile, Quantitative assessment of the risk of airborne transmission of SARS-CoV-2 infection: prospective and retrospective applications, Environ. Int. 145 (2020 Dec) 106112, https://doi.org/10.1016/j.envint.2020.106112. Epub 2020 Sep 6. PMID: 32927282; PMCID: PMC7474922.
[48] V. Stadnytskyi, C.E. Bax, A. Bax, P. Anfinrud, The airborne lifetime of small speech droplets and their potential importance in SARS-CoV-2 transmission, Proc. Natl. Acad. Sci. U. S. A. 117 (22) (2020 Jun 2) 11875–11877, https://doi.org/10.1073/pnas.2006874117. Epub 2020 May 13. PMID: 32404416; PMCID: PMC7275719.
[49] P.M. de Oliveira, L.C.C. Mesquita, S. Gkantonas, A. Giusti, E. Mastorakos, Evolution of spray and aerosol from respiratory releases: theoretical estimates for insight on viral transmission, Proc. Roy. Soc. A (2021), https://doi.org/10.1098/rspa.2020.0584, 4772020058420200584.
[50] G.R. Johnson, L. Morawska, Z.D. Ristovski, M. Hargreaves, K. Mengersen, C.Y. H. Chao, M.P. Wan, Y. Li, X. Xie, D. Katoshevski, S. Corbett, Modality of human expired aerosol size distributions, J. Aerosol Sci. 42 (Issue 12) (2011) 839–851, https://doi.org/10.1016/j.jaerosci.2011.07.009. ISSN 0021-8502.
[51] G.Y. Cao, H. Awbi, R.M. Yao, Y.Q. Fan, K. Siren, R. Kosonen, et al., A review of the performance of different ventilation and airflow distribution systems in buildings, Build. Environ 73 (2014) 171–186.
[52] N. Enberg, H. Alho, V. Loimaranta, M. Lenander-Lumikari, Saliva flow rate, amylase activity, and protein and electrolyte concentrations in saliva after acute alcohol consumption, Oral Surg. Oral Med. Oral Pathol. Oral Radiol. Endod. 92 (2001) 292–298.
[53] P. Khare, L.C. Marr, Simulation of vertical concentration gradient of influenza viruses in dust resuspended by walking, Indoor Air 25 (4) (2015 Aug) 428–440, https://doi.org/10.1111/ina.12156. Epub 2014 Oct 3. PMID: 25208212.
[54] K. Lin, C.R. Schulte, L.C. Marr, Survival of MS2 and Φ6 viruses in droplets as a function of relative humidity, pH, and salt, protein, and surfactant concentrations, PloS One 15 (12) (2020), https://doi.org/10.1371/journal.pone.0243505 e0243505. Published 2020 Dec 8.
[55] B. Jones, P. Sharpe, C. Iddon, E.A. Hathway, C.J. Noakes, S. Fitzgerald, Modelling uncertainty in the relative risk of exposure to the SARS-CoV-2 virus by airborne aerosol transmission in well mixed indoor air, Build. Environ. 191 (2021 Mar 15) 107617, https://doi.org/10.1016/j.buildenv.2021.107617. Epub 2021 Jan 19. PMID: 33495667; PMCID: PMC7816614.
[56] Yuguo Li, Hua Qian, Jian Hang, Xuguang Chen, Pan Cheng, Hong Ling, Shengqi Wang, Peng Liang, Jiansen Li, Shenglan Xiao, Jianjian Wei, Li Liu, Benjamin Cowling, Min Kang, Probable airborne transmission of SARS-CoV-2 in a poorly ventilated restaurant, Build. Environ. 196 (2021), https://doi.org/10.1016/j.buildenv.2021.107788, 107788.
[57] J.W. Cherrie, The effect of room size and general ventilation on the relationship between near and far-field concentrations, Appl. Occup. Environ. Hyg 14 (8) (1999 Aug) 539–546, https://doi.org/10.1080/104732299302530.PMID:10462849.